*Acta of Bioengineering and Biomechanics*
*Vol. 15, No. 2, 2013*

Original paper
DOI: 10.5277/abb130201

# Mechanical properties of the brain–skull interface

MOHAMMAD MYNUDDIN GANI MAZUMDER[1], KAROL MILLER[1]*, STUART BUNT[2], AHMED MOSTAYED[1], GRAND JOLDES[1], ROBERT DAY[3], ROBIN HART[4], ADAM WITTEK[1]

[1] Intelligent Systems for Medicine Laboratory, University of Western Australia, Australia.
[2] School of Anatomy, Physiology and Human Biology, University of Western Australia, Australia.
[3] Department of Medical Physics, Royal Perth Hospital, Perth, Australia.
[4] Department of Radiology, Royal Perth Hospital, Perth, Australia.

Knowledge of the mechanical properties of the brain-skull interface is important for surgery simulation and injury biomechanics. These properties are known only to a limited extent. In this study we conducted *in situ* indentation of the sheep brain, and proposed to derive the macroscopic mechanical properties of the brain–skull interface from the results of these experiments. To the best of our knowledge, this is the first ever analysis of this kind. When conducting *in situ* indentation of the brain, the reaction force on the indentor was measured. After the indentation, a cylindrical sample of the brain tissue was extracted and subjected to uniaxial compression test. A model of the brain indentation experiment was built in the Finite Element (FE) solver ABAQUS$^{TM}$. In the model, the mechanical properties of the brain tissue were assigned as obtained from the uniaxial compression test and the brain-skull interface was modeled as linear springs. The interface stiffness (defined as sum of stiffnesses of the springs divided by the interface area) was varied to obtain good agreement between the calculated and experimentally measured indentor force–displacement relationship. Such agreement was found to occur for the brain-skull interface stiffness of 11.45 $\frac{\mathrm{Nmm}^{-1}}{\mathrm{mm}^2}$. This allowed identification of the overall mechanical properties of the brain–skull interface.

*Key words*: *biomechanics, brain-skull, interface, mechanical properties, FEM*

## 1. Introduction

Recent developments in robotics technology, especially the emergence of automatic surgical tools and robots, accelerated the recent interest in brain tissue biomechanics for surgical simulation, computer-integrated and image-guided therapy, and as a supporting tool for diagnosis and prognosis of brain disease [1], [2]. For instance, a biomechanical model has been used to simulate the brain shift during neurosurgery for application requiring real time interaction involving large deformations, non-linear material properties and non-linear boundary conditions (BC). Craniotomy is an example of a surgical intervention during which brain–shift (movement of the brain) occurs due to known and unknown physical phenomena such as gravity, dural opening, surgical procedure, position of the patient during surgery, tissue behaviour and loss of Cerebrospinal Fluid (CSF).

A number of studies have been done to investigate the mechanical properties of brain tissue to model brain deformation for surgical inventions [3]–[15]. However, testing an isolated brain tissue is not adequate to develop a biomechanical model of human brain. The model should incorporate a boundary condition which is a realistic approximation of the nature of the brain–skull interaction. In the literature there is no consensus regarding the mechanical properties of the brain–skull interface. This is due to the fact that

* Corresponding author: Karol Miller, School of Mechanical and Chemical Engineering, University of Western Australia (M050) 35 Stirling Highway, Crawley, WA-6009 Australia. Tel: +6186488 8545, fax: +61864881024, e-mail: kmiller@mech.uwa.edu.au
Received: December 11th, 2012
Accepted for publication: February 5th, 2013

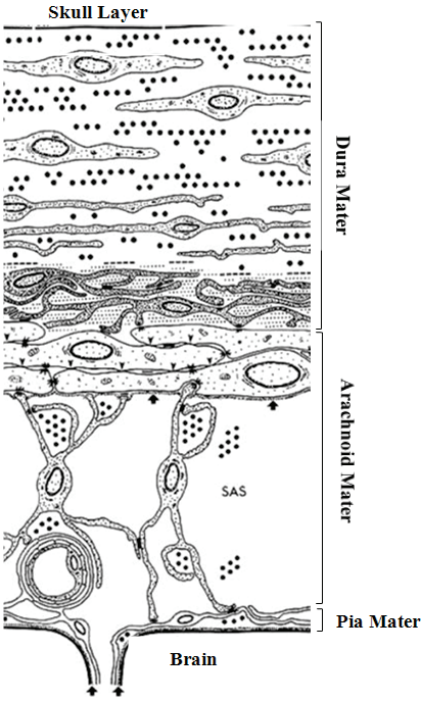


Fig. 1. Cranial Meninges (modified from Haines et al. [16])

very little has been known about the mechanical behaviour of the brain–skull interface. A detailed representation of the brain–skull interface is shown in Fig. 1 [16]. From the figure it can be seen that cranial meninges consists of three layers which are dura mater, arachnoid mater and pia mater.

The brain–skull interface models used in the literature are "best guesses" and their relation to reality is unclear [2]. Techniques used in the past to model the brain–skull interface include tied, frictionless or frictional sliding contact, with or without brain–skull separation [18]–[23]. The most straightforward way to determine the mechanical properties of the brain–skull interface would be to conduct experiments on interface samples. However, the exact anatomical structure of this interface is still a hotly debated topic, which is partly related to difficulties in extracting the interface samples without damaging tissues that form the interface [16]. Therefore, in this study we conduct *in situ* indentation of the sheep brain, and propose to derive the macroscopic mechanical properties of the brain–skull interface from the results of these experiments. To the best of our knowledge, this is the first ever analysis of this kind.

# 2. Materials and methods

When conducting *in situ* indentation of the brain, the reaction force on the indentor was measured. After the indentation, one cylindrical sample of brain tissue was extracted and subjected to uniaxial compression test to determine the subject-specific mechanical properties of the brain tissue. A model of the brain indentation experiment was built in ABAQUS$^{TM}$/Standard finite element solver [24]. In the model, the mechanical properties of the brain tissue were assigned to match those obtained from the uniaxial compression tests. The properties of the brain–skull interface were calibrated so that the calculated indentor reaction force and deformations within the brain matched those measured experimentally. The deformation field within the brain was verified by tracking the 3D motions of X-ray opaque marker implanted within the brain. This allowed identification of the overall mechanical properties of the brain–skull interface. The study scheme is shown in Fig. 2.

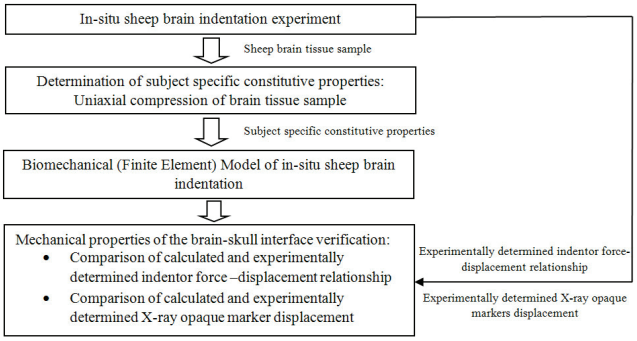


Fig. 2. Study scheme

## 2.1. *In situ* brain indentation experiment

Fresh sheep head from a 38 month old sheep was obtained from a local abattoir and kept at constant temperature 4 °C. The dissection started one hour prior to the experiment. A vibrating saw was used to make a 4 cm × 2 cm rectangular opening into the skull above the left hemisphere of the brain. A small cube of cortex close to its surface was removed using a scalpel. Thereafter, four X-ray opaque reference markers (diameter 1 mm) were placed at the four corners of the craniotomy area on the surface of the brain and these markers were then used to determine the location of the indentor during the experiment. Immediately after that five (5) X-ray opaque (spherical steel ball) markers (diameter 0.5 mm) were inserted using a stainless steel cannula (diameter .6 mm) into the brain in close proximity to the area of indentation. These markers were tracked by two OEC 9800 series mobile C-arms to determine the brain deformation. The whole system

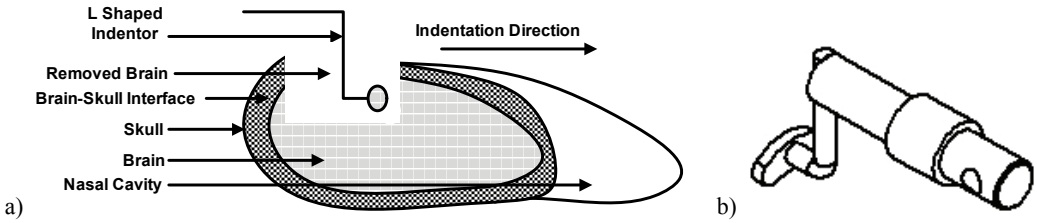


Fig. 3. (a) Schematic diagram of *in situ* sheep brain indentation and (b) L-shaped indentor

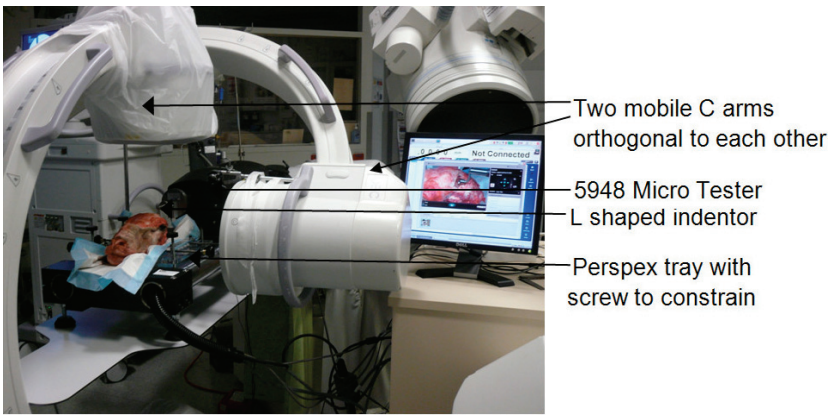


Fig. 4. Experimental set up for *in situ* brain indentation

consists of two image intensifiers and two sources. The OEC 9800 series by OEC Medical Systems Inc. Has a 12-inch tri-mode image intensifier with 1.6 lp/cm central resolution. The two mobile C-arms were positioned so that the imaging planes were orthogonal to each other and the images were captured at a rate of 2 frames per second and with a resolution of 1024 × 1024 pixels. A CT scan of the whole head was taken after specimen preparation which was later used for generating the 3D model of the sheep brain.

The 5948 Micro Tester Testing System was utilized for the *in situ* indentation experiment because of its versatility. For the experiment the horizontal configuration of the 5948 Micro Tester was used. The micromechanical system of Micro Tester 3948 consisted of a universal displacement actuator platform with a displacement control of 20 nm [25]. A special rectangular Perspex tray was used to constrain the sheep skull for tracking the markers implanted inside the brain during the experiment. An L-shaped indentor was used to indent the brain *in situ* in the craniotomy area. Schematic diagrams for the experiment and the L-shaped indentor are shown in Fig. 3.

The loading speed of the indentor was kept constant at 12 mm/min. The distance to maximum compression (the indentor displacement was measured from start of the contact between the indentor and the brain tissue until the indentor reached the maximum point of compression) was 4.8 mm. The whole experimental set up is shown in Fig. 4. To ensure a no-slip boundary condition, sand paper was attached on the face of the L-shaped indentor. It should be noted that prior to this experiment several trial experiments were conducted. Same protocols and methods were used to conduct these trials.

## 2.2. Determining subject specific material properties of the brain tissue

After the *in situ* brain indentation experiment the whole brain was extracted by dissecting the head using a vibrating saw. Then one cylindrical tissue sample was collected from the surface of the brain using a hollow stainless steel metal pipe (diameter 18 mm) with sharp edge. Because sheep brains are very small (five times smaller than the human brain), the cylindrical sample was collected from the other side of the brain to the side where *in situ* indentation was performed. The height of the sample was 12 mm approximately. The same Micro Tester 3948 was utilized vertically for the uniaxial compression test of sheep brain tissue. Following Miller and Chinzei [8], the constitutive properties of brain tissue were determined through semi-confined uniaxial compression of a tissue sample (see Fig. 5). During the experiment

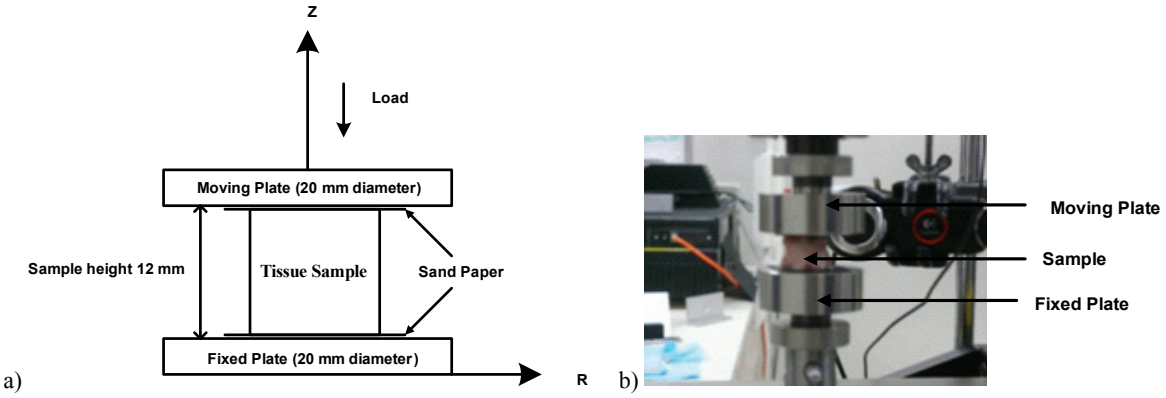


Fig. 5. Uniaxial compression test to determine material constants: (a) experiment set-up of the semi-confined uniaxial compression test, (b) uniaxial compression of brain tissue in vitro using 5948 Micro Tester

sand paper was glued to the surface of both the fixed plate and moving plate to maintain a no slip boundary condition. The loading speed was kept constant at 4 mm/min.

The brain tissue constitutive behaviour was modelled using an Ogden-type [26] Hyperelastic model as proposed by Miller and Chinzei [27]

$$W = \frac{2\mu}{\alpha^2}(\lambda_1^\alpha + \lambda_2^\alpha + \lambda_3^\alpha - 3) \qquad (1)$$

where: W – strain energy potential, $\lambda_i$ – principal stretches, $\mu$ – relaxed shear modulus, $\alpha$ – material coefficient. Constants $\mu$ and $\alpha$ of equation (1) were varied to obtain a calculated moving plate reaction force–time history close to the relationship measured from the experiments.

## 2.3. Determining the mechanical properties of the brain–skull interface

The geometry of the sheep brain was obtained through CT images. To distinguish the brain parenchyma from the skull and other tissues, the CT images were segmented using 3D SLICER (www.slicer.org), an open source software package for visualization and image analysis developed by Artificial Intelligence Laboratory of Massachusetts Institute of Technology and our collaborators in Surgical Planning Laboratory at Brigham and Women's Hospital and Harvard Medical School. As we found the sheep brain ventricles to be very small (of the order of 1 mm), we did not distinguish them in the segmentation. The mesh was built using IA-FEMesh [28] and HyperMesh (FE mesh generator by Altair of Troy, MI, USA). For FE discretisation, we used fully integrated hexahedral elements with hybrid formulation to prevent volumetric locking due to incompressibility of the brain tissue. Following Miller and Chinzei [27], the brain tissue was modelled as a homogenous Ogden-type Hyperelastic material with the constitutive constants determined from confined compression experiment as mentioned in Section 2.2.

The indentor and the skull were treated as rigid since they are orders of magnitude stiffer than the brain tissue. As mentioned in section 2.1 the position of the indentor was determined by using the four reference markers placed on the four surface corners of the brain. In order to model the interaction between the indentor and brain tissue, a contact interface model was introduced between the indentor (rigid body) and brain tissue (deformable body). For the contact between the front face of the indentor and the brain tissue, surface to surface hard contact formulations with augmented Lagrange constraint enforcement were applied [29]. A rough contact behaviour (no slip is allowed once the points are in contact) was used to represent the no-slip boundary condition between the soft tissue and indentor during the experiment.

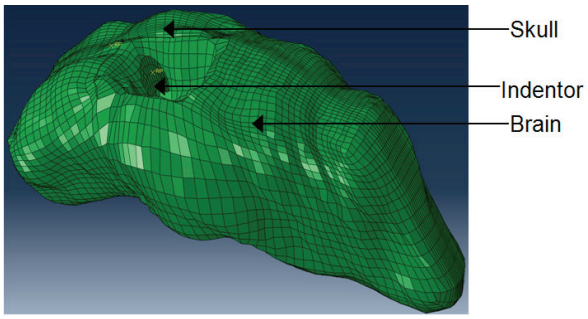


Fig. 6. ABAQUS™ model for the *in situ* brain indentation experiment (Brain: 25644 nodes and 22766 hexahedral elements; skull: 5241 nodes and 5208 rectangular shell elements; indentor – 1733 nodes and 3249 rectangular shell elements)

The loading was applied through prescribed motion of the reference point of the indentor mesh and with the constant speed of 12 mm/min. The skull nodes were rigidly constrained during the simulation.

We used the Full-Newton non-linear implicit dynamics solver available in ABAQUS$^{TM}$ FE code. The brain-skull interface was represented using 5240 linear elastic springs (0.3 mm length) connecting the nodes on the outer boundary of the brain model and skull (see Fig. 6).

## 2.4. Determining the brain deformation

The brain deformation was determined from the movement of the X-ray opaque markers. The indentor as well as the X-ray opaque markers were seen in the images captured by the mobile C-arms. To accurately determine the 3D displacements of the markers from the X-ray images, a correction of the geometrical distortion was performed by accounting for the radial and the tangential distortions.

The calibration of the mobile C-arm was done using a pinhole camera model in the same way as in Ma et al. [30]. The camera calibration method proposed by Zhang [31], [32] was utilized to calculate the camera parameters of the mobile C-arms. The camera parameters including the distortion coefficients were calculated using the camera calibration toolbox for Matlab [33]. Movement of the markers was tracked along the X-ray image sequences using codes implemented in Matlab (The Math Works, Natick, MA, USA). Firstly, the image boundaries were removed to choose the region of interest for the movement of the markers. A morphological gray scale filter was used to detect the markers from the X-ray images. The marker positions were highlighted in the image by performing a Top-hat Transform [34]. The disk shaped structuring element was used to locate the markers in the image. Subsequently, a thresholding was used to extract the marker location and the location of the markers was estimated as their centroid. Between two consecutive frames the tracking code only looked at the nearest neighbour location of a particular marker to track and update the position of the marker. It should be noted that the indentor location was determined using the four reference markers (1 mm diameter) placed on the surface of the brain in the area of the craniotomy as mentioned in Section 2.1. The location of the markers was available from the CT and X-ray images. The indentor location was estimated by performing registration of the two coordinate systems.

# 3. Results

## 3.1. Uniaxial compression test to determine the subject specific mechanical property

Figure 7 shows the comparison between the modelling and experimental results of force magnitude during uniaxial compression of the cylindrical brain tissue sample. For the analysed brain, Ogden type Hyperelastic material constants were determined as $\mu$ = 720 Pa and $\alpha$ = –4.7. For the determined subject specific material properties, the model accurately predicted indentor force–time history during the experiment.

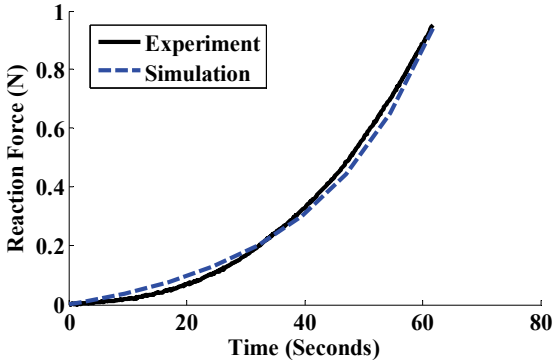


Fig. 7. Uniaxial compression of sheep brain tissue sample: comparison of modelling and experimental results of the indentor reaction force–time history

## 3.2. *In situ* indentation of sheep brain

Figure 8 shows the comparison between the calculated and experimentally measured indentor force–displacement relationship during the *in situ* brain

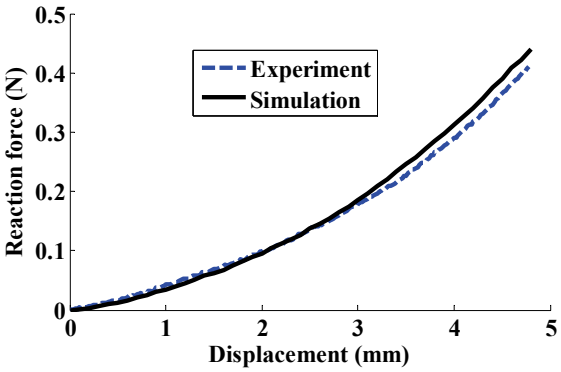


Fig. 8. Indentation of sheep brain *in situ*: comparison of modelling and experimental results

indentation. By using the subject specific material properties determined in the previous section and the linear springs representing the brain–skull interface, the model of *in situ* brain indentation accurately predicted indentor force–displacement relationship during the experiment. For indentation up to 4.8 mm, the error in force magnitude is less than 5%.

Figure 9 shows the trial experiment results from *in situ* indentation of the brain. The results from these trials were similar to the one we showed above.

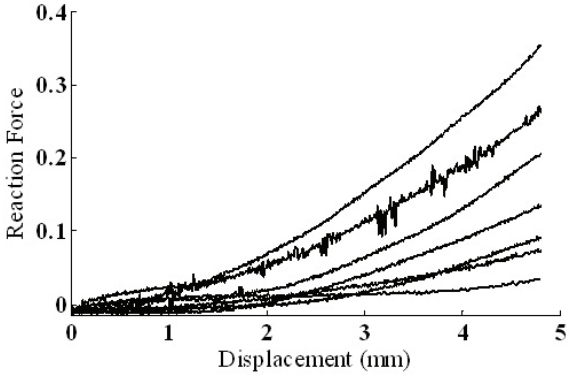


Fig. 9. Indentation of sheep brain *in situ*: experimental result for the reaction force–displacement relationship during trial experiments (each curve represents one experimental result)

## 3.3. Determination of the deformation field within the brain

In this section the comparison of the 3D displacements of the markers between the experimentally measured values and predicted modelling values are listed in Table 1. As the markers were not located at the vertices of the brain model mesh, the markers movement was computed from the nodal displacement using shape functions of the first order hexahedral element [35].

The maximum, minimum and average value of differences between experimentally measured displacement and predicted marker's displacement are listed Table 2. The average difference of displacement magnitude was 0.6 mm. The direction of marker movement indicates that the model predicted the brain deformation accurately (see Table 1).

## 3.4. Mechanical properties of the brain–skull interface

The brain–skull interface was represented using 5240 linear elastic springs (0.3 mm length) connecting the nodes on the outer boundary of the brain model (Fig. 6) and skull. The interface stiffness (defined as sum of stiffnesses of the springs divided by the interface area) was varied to obtain good agreement between the calculated (using the model summarized in Fig. 5) and experimentally measured indentor force–displacement relationship. Such agreement was found to occur for the brain–skull interface stiffness of 11.45 $\frac{\mathrm{Nmm}^{-1}}{\mathrm{mm}^2}$ (Fig. 8).

# 4. Discussion

In this study, we presented the results of experiments on sheep brain indentation in the area of the brain-skull interface and derived information about the

Table 1. Estimated marker displacements from the experiment and modelling

| Markers | Marker-1 | | Marker-2 | | Marker-3 | |
|---|---|---|---|---|---|---|
| Displacement in different coordinates | Modelling | X-ray image | Modelling | X-ray image | Modelling | X-ray image |
| *X* (mm) | –0.06 | –0.17 | 0.23 | 0.46 | 0.12 | 0.21 |
| *Y* (mm) | 0.61 | 1.09 | 0.41 | 0.88 | 0.31 | 0.61 |
| *Z* (mm) | 1.52 | 0.82 | 1.40 | 1.75 | 1.25 | 1.53 |

Table 2. Differences in marker displacements between the experiment and modelling

| Unit: mm | Maximum | Minimum | Average |
|---|---|---|---|
| Displacement in the *X* direction (mm) | 0.23 | 0.08 | 0.14 |
| Displacement in the *Y* direction (mm) | 0.47 | 0.29 | 0.41 |
| Displacement in the *Z* direction (mm) | 0.7 | 0.28 | 0.44 |
| Magnitude (mm) | 0.8 | 0.4 | 0.6 |

interface's mechanical properties by complementing analysis of the results of these experiments with brain modelling (using non-linear FE procedures).

Firstly, *in situ* indentation of sheep brain was conducted and the reaction forces on the indentor were measured. Subsequently, cylindrical sample of sheep brain was extracted and uniaxial compression test was conducted to determine the subject specific mechanical properties. Additionally, to determine the deformation field within the brain, two mobile C-arms were used to capture the displacements of the X-ray opaque markers planted within the brain. Calibration of the X-ray image intensifiers was done to correct any distortion present in the images. The 3D coordinates of the markers were triangulated from those images. Finally, a nonlinear Finite Element Model of the *in situ* indentation experiment was built in the FE solver ABAQUS$^{TM}$ and the properties of the brain-skull interface models were calibrated so that the calculated indentor reaction forces matched those measured experimentally. The 3D displacements of the X-ray opaque markers were obtained from the nodal displacements predicted by the FE model.

It was found that the developed Finite Element Model accurately predicts the force–displacement relationship of the indentor and 3D displacements of the implanted X-ray opaque markers that represent the local deformation of the brain (see Table 1). By representing the brain–skull interface as linear springs, we obtained good agreement between the calculated and the experimentally measured force–displacement relationship (see Fig. 8) and the brain–skull interface stiffness was determined as 11.45 $\frac{\mathrm{Nmm}^{-1}}{\mathrm{mm}^2}$. Although it can be regarded as a simple approach, linear springs have been previously used to represent the interface between the brain and skull for investigating injury biomechanics [36]–[38].

It is hypothesised that the minor differences between the experimental and modelling results observed in this study could be attributed to inaccuracies in determining the geometry of the brain. During the *in situ* sheep brain indentation experiment, the geometry of the sheep brain was obtained through CT images. After that segmentation was performed using 3D Slicer and at the end IA-FEMesh and Hypermesh were used to generate the brain mesh. The errors resulting from segmentation and mesh generation process contributed towards the discrepancies between the experimental and modelling results.

The results presented here are based on experimental studies. Therefore, one may expect several experiments to be conducted before establishing the modelling of the brain-skull interface. However, this is a first ever experiment of its kind. The preparation and method to conduct the experiment were very challenging as the equipments (CT and Mobile C arms) used during the experiment were primarily utilized for the patients in the hospital. Due to the complex setup of the experiment, seven *in situ* sheep brain indentation trial experiments were conducted before conducting the final experiment using CT and X-ray imaging. These trial experiments were conducted to check the repeatability of the experiment for *in situ* indentation (see Fig. 9).

Another limitation of our study is the number of specimens used to determine the subject specific material properties of the brain. We used only one cylindrical sample to determine the subject specific material properties of the brain due to small size of the sheep brain. Additionally, the model was verified by comparing the predicted displacement of the markers with those derived from the experiment. It should be noted that implanting markers inside the brain by using a cannula and a wire was an extremely difficult task. We tried to insert the markers in proximity area of indentation but it was not possible to track their position in real time. During the experiment two of the markers were occluded by the 5948 Micro Tester due to the complex setup of the equipments.

Despite some limitations, this study presents experimental results collected on *in situ* sheep brain indentation to determine the mechanical properties of the brain–skull interface with quantitative assessments of the brain deformation. The results presented here suggest that the brain–skull interface should be represented using linear springs of this stiffness rather than using sliding contact with no separation. More experimental work is necessary to validate the model of the brain–skull interface. One should be careful to extrapolate these results to human brain. Similar experimental and computational investigation for the human brain should be conducted.

## Acknowledgements

The first author of the paper was a Prescott scholar during this research. The financial support of the Australian Research Council (Discovery grant DP1092893), National Health and Medical Research Council (grant 1006031) and Medical and Health Research Infrastructure Fund of Western Australia in 2009–2011 is gratefully acknowledged.

## References

[1] OMMAYA A.K., *Mechanical Properties of Tissues of the Nervous System*, Journal of Biomechanics, 1968, Vol. 1, 127–138.

[2] MILLER K. (ed.), *Biomechanics of the Brain*, Springer New York, Dordrecht Heidelberg London, 2011, 117.

[3] FALLENSTEIN G.T., HULCE V.D., MELVIN J.W., *Dynamic Mechanical Properties of Human Brain Tissue*, Journal of Biomechanics, 1969, Vol. 2, 117–136.

[4] METZ H., MCELHANEY J., OMMAYA A.K., *A Comparison of the Elasticity of Live, Dead, and Fixed Brain Tissue*, Journal of Biomechanics, 1970, Vol. 3(4), 453–458.

[5] ESTES M.S., MCELHANEY J.H., *Response of Brain Tissue of Compressive Loading*, ASME, Paper No. 70, 1970.

[6] ARBOGAST K.B., MARGULIES S.S., *Regional Differences in Mechanical Properties of the Porcine Central Nervous System*, Proceedings of the 41st Stapp Car Crash Conference, 1997, SAE, 293–300.

[7] DONNELLY B.R., MEDIGE J., *Shear Properties of Human Brain Tissue*, Journal of Biomechanical Eng., 1997, Vol. 119(4), 423–432.

[8] MILLER K., CHINZEI K., *Constitutive Modelling of Brain Tissue: Experiment and Theory*, Journal of Biomechanics, 1997, Vol. 30, 1115–1121.

[9] ARBOGAST K.B., MARGULIES S.S., *Material Characterization of the Brainstem from Oscillatory Shear Tests*, Journal of Biomechanics, 1998, Vol. 31(9), 801–807.

[10] BRANDS D.W.A., BOVENDEERD P.H.M., PETERS G.W.M., WISMANS J.S.H.M., *The Large Shear Strain Dynamic Behaviour of In-Vitro Porcine Brain Tissue and the Silicone Gel Model Material*, Proceedings of the 44th Stapp Car Crash Conference, 2000, 44, 249–260.

[11] PRANGE M.T., MARGULIES S.S., *Regional, Directional and Age-Dependent Properties of Brain Undergoing Large Deformation*, Journal of Biomechanical Engineering, 2002, Vol. 124, 244–252.

[12] BILSTON L.E., LIU Z., PHAN-THIEN N., *Linear Viscoelastic Properties of Bovine Brain Tissue in Shear*, Biorheology, 1997, Vol. 34(6), 377–385.

[13] BILSTON L. E., LIU Z., PHAN-THIEN N., *Large Strain Behavior of Brain Tissue in Shear: Some Experimental Data and Differential Constitutive Model*, Biorheology, 2001, Vol. 38(4), 335–345.

[14] HRAPKO M., VAN DOMMELEN J.A., PETERS G.W., WISMANS J.S., *The Mechanical Behaviour of Brain Tissue: Large Strain Response and Constitutive Modelling*, Biorheology, 2006, Vol. 43(5), 623–636.

[15] VELARDI F., FRATERNALI F., ANGELILLO M., *Anisotropic Constitutive Equations and Experimental Tensile Behavior of Brain Tissue*, Biomechanics and Modeling in Mechanobiology, 2006, Vol. 5, 53–61.

[16] HAINES D.E., HARKEY H.L., AL-MEFTY O., *The "Subdural" Space: A New Look at an Outdated Concept*, Journal of Neurosurgery, 1993, Vol. 32, 111–120.

[17] JIN X., *Biomechanical Response and Constitutive Modeling of Bovine Pia-Arachnoid Complex*, Wayne State University PhD thesis, 2009.

[18] HU J., JIN X., LEE J.B., ZHANG L., CHAUDHARY V., GUTHIKONDA M., YANG K.H., KING A.I., *Intraoperative Brain Shift Prediction Using a 3D Inhomogeneous Patient-Specific Finite Element Model*, Journal of Neurosurgery, 2007, Vol. 106, 164–169.

[19] JI S., MARGULIES S., *Brainstem Motion Within the Skull: Measurement of the Pons Displacement In Vivo*, Journal of Biomechanics, 2007, Vol. 40(1), 92–99.

[20] MIGA M.I., PAULSEN K.D., HOOPES P.J., KENNEDY F.E., HARTOV A., ROBERTS D.W., *In Vivo Modelling of Interstitial Pressure in the Brain Under Surgical Load Using Finite Elements*, Journal of Biomechanical Engineering, 2000, Vol. 122(4), 354–363.

[21] WITTEK A., OMORI K., *Parametric Study of Effects of Brain–Skull Boundary Conditions and Brain Material Properties on Responses of Simplified Finite Element Brain Model Under Angular Acceleration Impulse in Sagittal Plane*, JSME International Journal Series C, 2003, Vol. 46(4), 1388–1399.

[22] WITTEK A., KIKINIS R., WARFIELD S.K., MILLER K., *Brain Shift Computation Using a Fully Nonlinear Biomechanical Model*, Proceedings of the 8th International Conference on Medical Image Computing and Computer-Assisted Intervention (MICCAI) LNCS, 2005, Vol. 8(2), 583–590.

[23] WITTEK, A., MILLER K., KIKINIS R., WARFIELD S.K., *Patient-Specific Model of Brain Deformation: Application to Medical Image Registration*, Journal of Biomechanics, 2007, 40, 919–929.

[24] ABAQUS I., ABAQUS Online Documentation: Version 6.7-1, 2007.

[25] Instron, Documentation of 5948 MicroTester Ultra-High Precision System for Mechanical Testing, (available from: http://www.instron.us/wa/product/MicroTester-System-for-Low-Force-Static.aspx?ref=http://www.google.com.au/url)

[26] OGDEN R.W., *Large deformation isotropic elasticity – On the Correlation of Theory and Experiment for Incompressible Rubberlike Solids*, Proceedings of the Royal Society of London, Series A, Mathematical and Physical Sciences, 1972, Vol. 326, 565–584.

[27] MILLER K., CHINZEI K., *Mechanical Properties of Brain Tissue in Tension*, Journal of Biomechanics, 2002, Vol. 30, 1115–1121.

[28] MAGNOTTA V., LI W., GROSLAND N., *Comparison of Displacement-Based and Force-Based Mapped Meshing*, Workshop on Computational Biomechanics for Medicine at MICCAI, Insight Journal, 2008.

[29] ABAQUS/CAE User's manual, ABAQUS Online Documentation: Version 6.10, 2010.

[30] MA J., W. A., SINGH S., JOLDES G., WASHIO T., CHINZEI K., MILLER K., *Evaluation of Accuracy of Non-Linear Finite Element Computations for Surgical Simulation: Study Using Brain Phantom*, Computer Methods in Biomechanics and Biomedical Engineering, 2010, Vol. 13(6), 783–794.

[31] ZHANG Z., *Flexible Camera Calibration by Viewing a Plane from Unknown Orientations*, Proceedings of International Conference on Computer Vision in Greece, 1999.

[32] ZHANG Z., *A Flexible New Technique for Camera Calibration*, IEEE Transactions of Pattern Analysis and Machine Intelligence, 2000, Vol. 22(11), 1330–1334.

[33] BOUGUET J.Y., *Documentation of a complete Camera Calibration Toolbox for Matlab* [Internet], California Institute of Technology, (c) 1999–2008, (cited 2009 May 19, available from: http://www.vision.caltech.edu/bouguetj/index.html).

[34] SOLOMON C., BRECKON T., LOGAN L.D., *Fundamentals of Digital Image Processing*, Willey-Blackwell, 2011, 230–231.

[35] LOGAN L.D., *A First Course in the Finite Element Method*, Brooks/Cole, 2002, 430–432.

[36] COATS B., STEPHANIE A.E., SULLIVAN S., MARGULIES S.S., *Finite Element Model Predictions of Intracranial Hemorrhage from Non-Impact, Rapid Head Rotations in the Piglet*, International Journal of Developmental Neuroscience, 2012, Vol. 30(3), 191–200.

[37] BAGHAEI S.M., SADEGH A.M., RAJAAI S.M., *An Analytical Model for Investigating the Role of Meningeal Interfaces in the Brain Motion Relative to the Skull in Low-Velocity Head Impacts*. International Journal of Biomedical Engineering Technology, 2011, Vol. 5(1), 61–67.

[38] FENG Y., ABNEY T.M., OKAMOTO R.J., PLESS R.B., GENIN G.M., BAYLY P.V., *Relative Brain Displacement and Deformation During Constrained Mild Frontal Head Impact*, Journal of Royal Society Interface, 2010, Vol. 7(53), 1677–1688.